Geomagnetic Field Model Indicates Shrinking Northern Auroral Oval

Bruno Zossi, Mariano Fagre, Hagay Amit, Ana Elias

▶ **To cite this version:**

Bruno Zossi, Mariano Fagre, Hagay Amit, Ana Elias. Geomagnetic Field Model Indicates Shrinking Northern Auroral Oval. Journal of Geophysical Research Space Physics, 2020, 125 (8), 10.1029/2019JA027434 . hal-02915580

HAL Id: hal-02915580
https://hal.science/hal-02915580

Submitted on 25 Jun 2022

HAL is a multi-disciplinary open access archive for the deposit and dissemination of scientific research documents, whether they are published or not. The documents may come from teaching and research institutions in France or abroad, or from public or private research centers.

L'archive ouverte pluridisciplinaire **HAL**, est destinée au dépôt et à la diffusion de documents scientifiques de niveau recherche, publiés ou non, émanant des établissements d'enseignement et de recherche français ou étrangers, des laboratoires publics ou privés.

Copyright

Check for updates

JGR Space Physics

RESEARCH ARTICLE
10.1029/2019JA027434

Geomagnetic Field Model Indicates Shrinking Northern Auroral Oval

Bruno Zossi[1,2], **Mariano Fagre**[2,3], **Hagay Amit**[4], **and Ana G. Elias**[1,2]

[1]INFINOA (CONICET-UNT) and Laboratorio de Física de la Atmosfera, Departamento de Física, Facultad de Ciencias Exactas y Tecnología, Universidad Nacional de Tucuman, San Miguel de Tucuman, Argentina, [2]Consejo Nacional de Investigaciones Científicas y Técnicas, CONICET, San Miguel de Tucuman, Argentina, [3]Laboratorio de Telecomunicaciones, Departamento de Electricidad, Electrónica y Computación, Facultad de Ciencias Exactas y Tecnología, Universidad Nacional de Tucuman, San Miguel Tucuman, Argentina, [4]Laboratoire de Planétologie et de Géodynamique, CNRS, Université de Nantes, Nantes Atlantiques Universités, Nantes, France

Key Points:
- During 1900–1940 the modeled area of polar caps and auroral ovals increased consistent with the geomagnetic dipole moment decrease
- During 1940–2015 the southern auroral oval area continued to increase while the northern has been decreasing rapidly
- This hemispherical dichotomy is related to asymmetry in the core field and its secular variation

Supporting Information:
- Supporting Information S1
- Table S1

Correspondence to:
B. Zossi,
bzossi@herrera.unt.edu.ar

Citation:
Zossi, B., Fagre, M., Amit, H., & Elias, A. G. (2020). Geomagnetic field model indicates shrinking northern auroral oval. *Journal of Geophysical Research: Space Physics*, *125*, e2019JA027434. https://doi.org/10.1029/2019JA027434

Received 19 SEP 2019
Accepted 27 MAY 2020
Accepted article online 29 JUL 2020

Abstract Polar cap and auroral oval areas are presented for the period 1900–2015 using a model of the magnetosphere and the International Geomagnetic Reference Field Version 12 (IGRF-12) model for the geomagnetic field. The effect of the main field long-term changes is addressed considering steady interplanetary conditions. Until ~1940 both northern and southern polar cap areas increased with time, consistent with the geomagnetic dipole moment decrease during this period. Thereafter, while the southern polar cap area continued to increase steadily, the northern polar cap area has been decreasing rapidly. This hemispherical dichotomy is related to asymmetry in the core field and its secular variation. In the southern polar region the surface field intensity has been decreasing throughout the entire period, whereas in the northern polar region an intensity decrease turned to an increase from 1940 to present day. This recent surface intensity increase stems from intensification of the flux patch below Siberia and cessation of weakening of the flux patch below North America, both on the core-mantle boundary. The surprising temporal decrease in the area of the northern polar cap has important implications for space weather and communication systems. While the decreasing dipole intensity allows more particles to penetrate the atmosphere, a shrinking northern auroral oval implies an increase in particle precipitation density, resulting in more severe damage to airplanes and ships positioning systems, spacecraft electronic systems and airline passengers when passing above this region. Further study is needed to observationally establish that the northern auroral oval, as defined by optical occurrences of aurora, is indeed shrinking.

Plain Language Summary Auroral ovals are bands encircling polar caps where particles from the Sun are accelerated down into the atmosphere. Their area and location depend on the Earth's magnetic field and solar wind conditions. The Earth's field, which is mainly dipolar, varies gradually in time, producing a slow shift in the geographic location of the auroral oval, moving with it the locations where auroras can be seen. Based on the geomagnetic dipole moment decrease in the last century, it was expected that the auroral ovals would drift in equatorial direction and embrace more area in time. In this work we show, using three different models, how the polar cap and auroral oval areas in both hemispheres changed from 1900 to 2015. While southern areas increase as expected from a dipolar moment decrease, northern areas have been decreasing since ~1940. This surprising decrease has important implications for space weather and communication systems. The allowance of more energetic particles to the atmosphere due to the decreasing dipole intensity is reinforced by a shrinking northern auroral oval that implies an increase in particle precipitation density, resulting in more severe damage to positioning and spacecraft electronic systems, and airline passengers when passing above this region.

1. Introduction

Auroral ovals are belts where particles carried by the solar wind are accelerated down the magnetic field lines onto the upper atmosphere (Akasofu, 1983; Feldstein, 2016). Directly linked to auroral ovals are polar caps, which are regions above Earth's surface where magnetic field lines are open and connected to the interplanetary magnetic field. Their border is also called open-closed field line boundary since it separates open magnetic field lines from the closed lines of the magnetosphere. Polar cap geometry, that is, center, shape, and area, can be determined by identifying and following these open field lines using mathematical

©2020. American Geophysical Union. All Rights Reserved.

modeling that can range in complexity from magnetohydrodynamic (Gombosi et al., 2004) to simplified fast models (Hill & Rassbach, 1975; Stern, 1973). These features depend directly on the morphology of the magnetosphere, which in turn depends on Earth's magnetic field and solar wind conditions.

Auroral ovals are vulnerable to particle precipitation effects. A relevant problem in these areas is the "blackout" of ionospherically propagating radio signals affecting communications as well as satellite geolocation, fundamental for airplanes and ships positioning systems. Among other consequences of particle precipitation are changes in atmosphere chemistry with dissociation of ozone possibly the worst of these alterations (Glassmeier & Vogt, 2010; Winkler et al., 2008), degradation of spacecraft electronic systems and components (Carlowicz & Lopez, 2002; Olson & Amit, 2006), and radiation effects that might be hazardous to passengers, crew, and equipment in transpolar flights (Riley et al., 2018).

Earth's magnetic field at present is dominated by a dipole with its axis tilted about 11° with respect to the Earth rotation axis, that is, the field is almost perpendicular to the solar wind flow direction. In contrast, the temporal variability of the field, termed secular variation (SV), is characterized by a blue spectrum; that is, its power increases with increasing spherical harmonic degree from weakest dipole SV power to stronger for larger degrees (Lowes, 1974). SV timescales for the nondipole field are inversely proportional to the degree (Amit et al., 2018; Christensen & Tilgner, 2004; Lhuillier et al., 2011). The most striking SV features are westward drifting low- and middle-latitude flux patches in the Atlantic hemisphere (e.g., Finlay & Jackson, 2003; Jackson et al., 2000), which were modeled by control of inner core boundary conditions on the geodynamo (Aubert et al., 2013). The SV may be inverted for fluid motions at the top of the core (e.g., Holme, 2015). These core flow models often include a large-scale anticlockwise eccentric gyre below the Atlantic hemisphere with high level of equatorial symmetry (Finlay et al., 2016; Gillet et al., 2019) in agreement with theoretically expected dominant rotational effects (e.g., Busse, 1970; Jault, 2008).

The SVs of the auroral ovals were studied previously with focus on solar activity, which is a strong forcing of auroral ovals and auroral occurrence frequency as well. Silverman (1992) defined auroral occurrence as the number of days in which aurora was observed in a given time interval, and the SV analyzed is that associated to the solar activity. He used visual auroral observations for an ~500-yr period from 1450 to 1948 together with sunspot and the geomagnetic aa index from 1868 to 1990, comparing SV when possible. Silverman (1992) found an anticorrelation of auroral occurrence in polar regions with solar activity, which he attributed to the auroral oval displacement due to solar and geomagnetic activity variations. Korte and Stolze (2016) studied the effects of the geomagnetic dipole moment (intensity and tilt) and solar activity. They used archeomagnetic field models that span several millennia. Korte and Stolze (2016) concluded that the main forcings of midlatitude aurora occurrence likelihood and the spatial extent of the auroral zone at multidecadal to centennial timescales are the geomagnetic tilt and solar activity. Most importantly however, both Silverman (1992) and Korte and Stolze (2016) did not consider the effect of the nondipolar components.

The SV of the geomagnetic field affects the magnetosphere and consequently polar cap and auroral oval characteristics. In this work, for the first time, the SV of the polar cap and auroral oval areas are calculated. We investigate this SV for the period 1900–2015 using a model of the magnetosphere and a geomagnetic field model inferred from surface and satellite observations. The effect of the main field long-term changes is addressed by considering steady interplanetary conditions.

2. Methodology

2.1. Magnetosphere Boundary Models

To determine polar cap boundaries, centers, and areas, we considered a theoretical magnetosphere boundary model. We estimated the outer limit of the magnetosphere by balancing the dynamic pressure of the solar wind and the magnetic pressure of the geomagnetic field (Beard, 1960), that is,

$$\left(2\rho v^2 \cos^2\psi\right)_{sw} = \left(\frac{B^2}{2\mu_0}\right)_{mf} \tag{1}$$

where ρ is the proton density, v the solar wind velocity, ψ the angle between solar wind direction and magnetopause limit, B the magnetic field intensity, μ_o the magnetic permeability and the subscripts "sw" and "mf" denote solar wind and Earth's magnetic field, respectively. Mean solar wind values for quiet

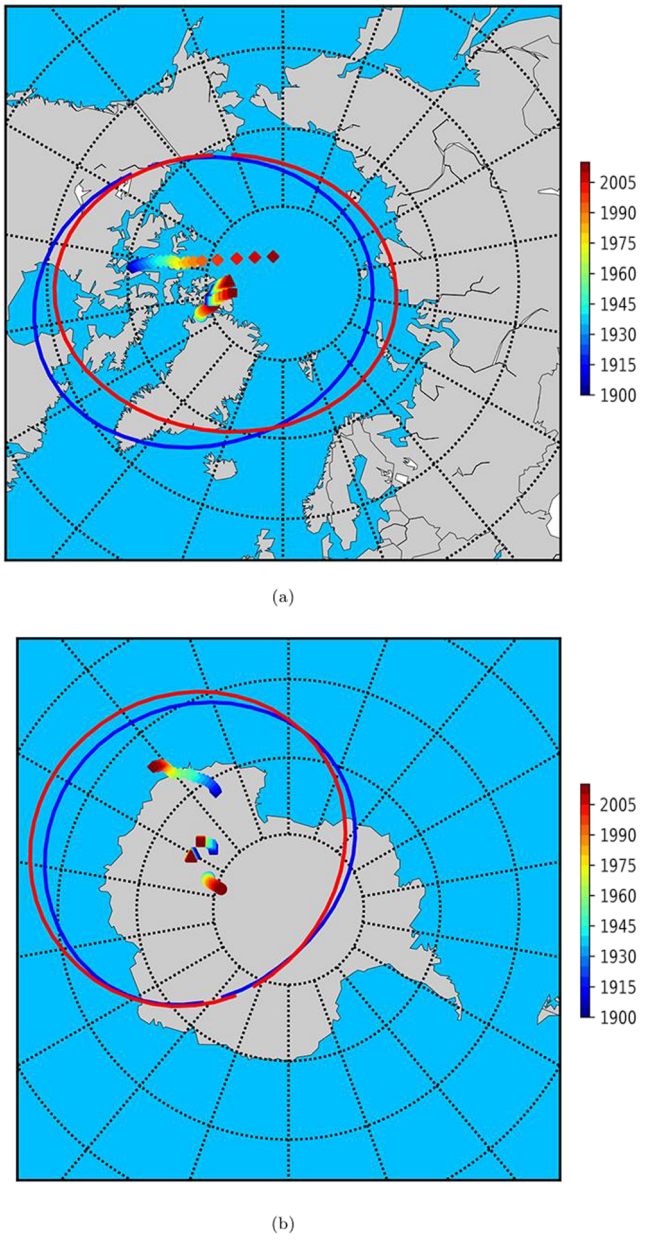

Figure 1. (a) Northern and (b) southern polar cap boundaries obtained with 2-D convex hull for 1900 (blue) and 2015 (red), with magnetic poles (diamonds), centered (circles) and eccentric (triangles) dipole axes, and polar cap geometric centers (squares) from 1900 (blue) to 2015 (red) in 5-yr intervals. The year corresponding to each symbol is denoted by colors (see color bar).

conditions $\rho \approx 4.2 \times 10^{-21}$ kg m^{-3} and $v = 350$ km/s yield $B = 49$ nT, corresponding to 10.8 R_E, with $R_E = 6{,}371$ km the mean Earth radius. The surface in space where $B = 49$ nT serves as a magnetopause model, which we term the "constant intensity" model. That is, the magnetic field at every point of the magnetopause is 49 nT since this value is determined by the solar wind dynamic pressure, which we consider fixed for all the cases analyzed. This intensity value would occur at different positions depending on the field configuration. Every line between 90° inclination and the line with $B = 49$ nT at its apex is cut by this surface and is therefore considered as an "open field line". Polar caps are located and delineated by following open field lines and tracing them to the Earth surface. This serves as the inner limit of auroral ovals. The outer limit is assessed similarly by considering disturbed solar wind conditions with $\rho \approx 5.0 \times 10^{-21}$ kg m^{-3}and $v = 500$ km/s, consistent with typical values during low to moderate perturbations.

A second model of the open field lines can be obtained by the superposition of the Earth's field of core origin and a uniform field in the direction of the interplanetary external field (Hill & Rassbach, 1975), as was done in Zossi et al. (2019). With this model it is possible to obtain the polar cap location by calculating the neutral magnetic field points ($B = 0$) and following the lines down to the Earth surface. Neutral points separate the open and closed magnetic field lines.

In contrast to the two first principle models described above, a third semi-empirical magnetosphere Model T04 (Tsyganenko & Sitnov, 2005) is obtained with conditions considered in Tsyganenko (2019). This model provides a good assessment of magnetospheric magnetic field, using full International Geomagnetic Reference Field (IGRF) for the internal field and based on satellite observations that account for the contributions from external magnetospheric sources as the ring current, magnetotail current system, magnetopause currents, and large-scale system of field-aligned currents. Tsyganenko (2019) defined the auroral zone location as the lines that cross inside two quasi circles on the ecliptic plane. The outer circle defines the polar cap.

The three models span different altitude ranges. The "constant intensity" model is valid from the magnetopause down to the Earth's surface. The magnetosphere field is that of the IGRF without any deformations in the entire region. The "superposition" model is valid in the entire space, below and above the magnetopause. T04 model gives a more precise shape of the magnetospheric lines approaching the magnetopause. Although the magnetic field differences among the three models are large close to the magnetopause, these models converge on approach to the Earth *surface*. None of the three models simulate the magnetosphere-ionosphere coupling.

2.2. Areas and Centers of Polar Caps

Magnetic field lines were traced using the same algorithm as in Zossi et al. (2019). Briefly, if the magnetic field $B = (Bx, By, Bz)$ is known at every point then the magnetic field line element $dl = (dx, dy, dz)$ is defined by the following equation

$$\frac{dx}{B_x} = \frac{dy}{B_y} = \frac{dz}{B_z} \tag{2}$$

which is solved with a fourth-order Runge-Kutta method. The lines cut by our modeled magnetopause were traced then to the Earth surface. A 2-D convex hull routine (Schneider & Eberly, 2003) was used

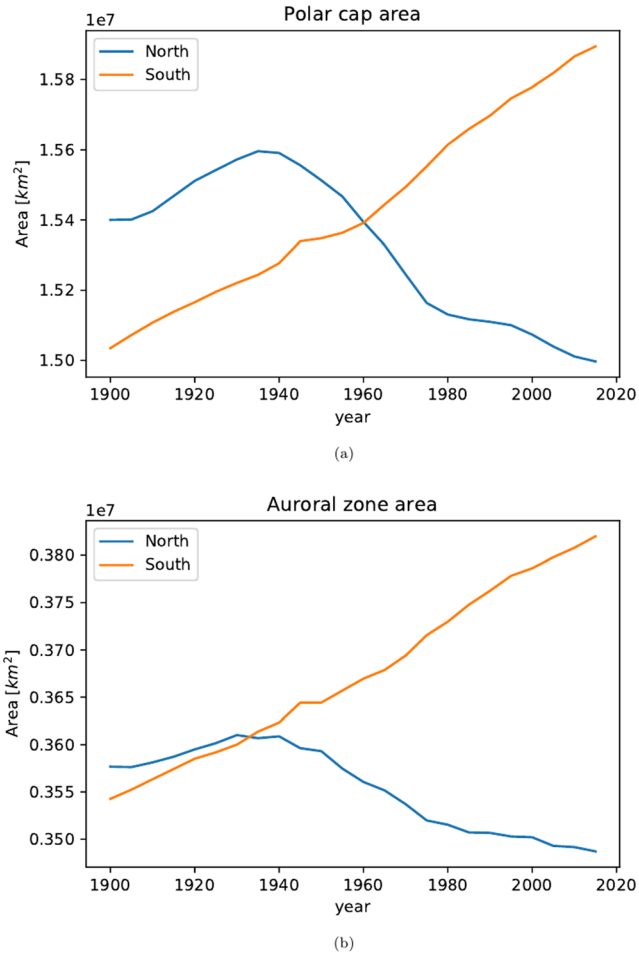

Figure 2. Secular variation of northern (blue) and southern (orange) polar cap (a) and auroral oval (b) areas, both estimated using maximum degree 5 in IGRF-12 magnetic scalar potential expansion.

to draw the boundary in terms of geographic latitude and longitude, as can be seen in Figure 1 for 1900 and 2015.

For Earth's magnetic field, the IGRF Version 12 model (Thébault et al., 2015) was used considering maximum spherical harmonic degree and order 5 in the magnetic scalar potential expansion. The choice of truncation level was based on a convergence analysis estimating polar cap areas versus the truncation degree. As can be seen in Figure 2, polar cap areas approach asymptotic values already when truncated at degree 3. Areas estimated using until degree 5 differ by less than 0.1% from estimations using until degree 4. Adding higher degrees differ by less than this value. This truncation affects even less the field lines at the magnetopause height since the field decreases with $r^{-(n+1)}$, that is, very rapidly with radial distance.

Areas were calculated using the formula for a polygon on the surface of a sphere formed by the arcs of great circles joining these boundary points, that is (Bevis & Cambareri, 1987), $A_{\text{polygon}} = [\theta - (n-2)\pi]R_E^2$, where θ is the sum of the inner angles of the spherical polygon on the Earth surface and n the number of sides. To verify the reliability of the area estimation, we compared it with the known analytical solution for the area of the polar cap for an axial dipole field, which is $A_{\text{analytical}} = 2\pi\, R_E^2\, [1 - \cos(90 - \lambda_P)]$ (from a spherical cap area equation), where λ_P is the axisymmetric polar cap boundary latitude. For this case, considering mean solar wind conditions, $\lambda_P = \pm 72°$. The ratio of the analytical to the estimated polar cap area using the "constant intensity" model is $A_{\text{polygon}}/A_{\text{analytical}} = 1.0006$, that is, a very good agreement.

Polar cap centers were obtained by projecting polar cap points to a plane using "Lambert azimuthal equal-area projection", averaging the Cartesian components and converting back the center Cartesian coordinates to geodetic spherical coordinates. These polar cap geometric centers were compared with magnetic dip poles, and with centered and eccentric geomagnetic dipole axes (Fraser-Smith, 1987). The magnetic dip poles correspond to the places on the Earth's surface where the magnetic field inclination is 90°. The geomagnetic dipole axis longitude ϕ_{cd} and colatitude θ_{cd} are given by the commonly used centered spherical harmonic coefficients of degree 1 (e.g., Amit & Olson, 2008):

$$\phi_{cd} = \tan^{-1}\left(\frac{h_1^1}{g_1^1}\right) \tag{3}$$

$$\theta_{cd} = \tan^{-1}\left(\frac{\sqrt{g_1^{1^2} + h_1^{1^2}}}{g_1^0}\right) \tag{4}$$

where ${g_1}^0$ represents the axial dipole and ${g_1}^1$ and ${h_1}^1$ represent the equatorial dipole. The eccentric dipole axis coordinates ϕ_{ed} and θ_{ed} are given by the corresponding dipole coefficients in a reference system off Earth's center. In terms of the centered spherical harmonic coefficients, the eccentric dipole axis coordinates are (e.g., Fraser-Smith, 1987)

$$\phi_{ed} = \tan^{-1}\left[\frac{(R_E \mp \Delta z)\sin\phi_{cd}\tan\theta_{cd} \pm \Delta y}{(R_E \mp \Delta z)\sin\phi_{cd}\tan\theta_{cd} \pm \Delta x}\right] (-\text{north}, +\text{south}) \tag{5}$$

$$\begin{aligned}\theta_{ed} &= \sin^{-1}\left[\frac{\Delta x\sin\phi_{cd} - \Delta y\cos\phi_{cd}}{R_E\sin(\phi_{cd} - \phi_{ed})}\right] (\text{north}),\ \theta_{ed} \\ &= 180° - sin^{-1}\left[\frac{\Delta x\sin\phi_{cd} - \Delta y\cos\phi_{cd}}{R_E\sin(\phi_{cd} - \phi_{ed})}\right] (\text{south})\end{aligned} \tag{6}$$

where $\Delta z = [(L_0 - {g_1}^0 E)/3{B_o}^2]R_E$, $\Delta x = [(L_1 - {g_1}^1 E)/3{B_o}^2]R_E$, $\Delta y = [(L_2 - {h_1}^1 E)/3{B_o}^2]R_E$,

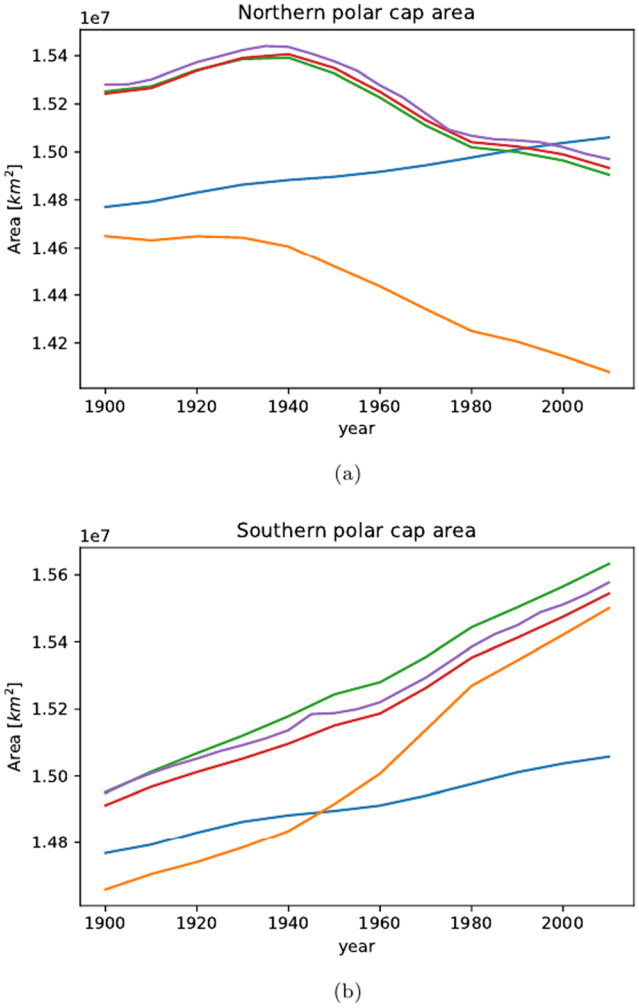

Figure 3. Secular variation of (a) northern and (b) southern polar cap areas estimated using maximum spherical harmonic degree 1 (blue), 2 (orange), 3 (green), 4 (red), and 5 (purple) using the IGRF-12 magnetic scalar potential expansion.

$L_0 = 2{g_1}^0{g_2}^0 + 3^{1/2}({g_1}^1{g_2}^1 + {h_1}^1{h_2}^1)$, $L_1 = -{g_1}^0{g_2}^0 + 3^{1/2}({g_1}^0{g_2}^1 + {g_1}^1{g_2}^1 + {h_1}^1{h_2}^2)$, $L_2 = -{h_1}^1{g_2}^0 + 3^{1/2}({g_1}^0{h_2}^1 - {h_1}^1{g_2}^2 + {g_1}^1{h_2}^2)$, $E = (L_0{g_1}^0 + L_1{g_1}^1 + L_2{h_1}^1)/4{B_o}^2$, and ${B_o}^2 = ({g_1}^0)^2 + ({g_1}^1)^2 + ({h_1}^1)^2$.

Note that we relied on the standard eccentric dipole definition based on the dipole (${g_1}^0$, ${g_1}^1$, ${h_1}^1$) and quadrupole (${g_2}^0$, ${g_2}^1$, ${g_2}^2$, ${h_2}^1$, ${h_2}^2$) Gauss coefficients of the geomagnetic field spherical harmonics (Fraser-Smith, 1987), while Tsyganenko (2019) considered a somewhat modified eccentric dipole definition based on the full IGRF.

3. Results

Figure 1 shows the SV of geometric centers of polar caps (squares). For comparison, we also track the centered (circles) and eccentric (triangles) geomagnetic dipole axis and the magnetic dip poles (diamonds). We find that the motions of the centers are adequately explained by the eccentric dipole axis SV, whereas the centered dipole is slightly shifted and the magnetic poles move much faster. This is in agreement with Tsyganenko (2019) who found that the auroral ovals follow the geomagnetic eccentric dipole instead of the magnetic dip poles. In addition, Figure 1 confirms the hemispherical dichotomy in the polar caps SV with faster motion in the north, again in agreement with Tsyganenko (2019).

The absolute SVs of each polar cap (northern and southern) for the period 1900–2015, shown in Figure 2a, are mostly larger than those expected for a pure dipole field (compare purple and blue lines of Figure 3). In addition, an increase can be noticed until ~1940 in both cases, which is qualitatively consistent with the expected increase in area due to the geomagnetic dipole moment decrease during the historical period. Quantitatively, however, both the northern and the southern polar cap areas increased during that period faster than if a pure dipole field prevailed. Thereafter, while the southern polar cap continued to increase steadily, the northern polar cap switched to an abrupt and fast decrease until ~1980 followed by a somewhat less steep decrease until present day (blue line in Figure 2a). In percentage terms, we find an average rate of ~0.05%/yr increase in the southern case during the period 1900–2015, as opposed to an ~0.01%/yr increase during 1900–1940 followed by an ~0.03%/yr decrease during 1940–2015 in the northern case. For comparison, the geomagnetic dipole has been decreasing at a rate of ~0.05%/yr (e.g., Finlay et al., 2016). If this trend persists linearly, the northern polar cap might vanish within less than 4,000 yr.

Auroral oval areas were determined by subtracting polar cap areas from those obtained considering the disturbed solar wind conditions. Their SV is in good agreement with that of polar cap areas (compare Figures 2a and 2b). Similar results are obtained for polar cap and auroral oval areas using the other two magnetosphere models.

The SV of polar caps obtained with the constant intensity magnetopause model is in reasonable agreement with the two additional models (Figure 4) despite relying on different assumptions (Tsyganenko, 2019; Zossi et al., 2019). The polar caps boundary definition in the superposition model is somewhat noisier than in the other two models. However, the general trends of all three models exhibit a steady decrease in the south as opposed to increase/decrease before/after 1940 in the north, with the models differing mostly by a constant. This constant difference arises due to the differences in the coordinates from where the open field lines are identified in each model. In the constant intensity model this boundary depends on the dynamic solar wind pressure value. In the superposition model, which does not have a defined boundary, the open field lines depend on the value of the uniform external magnetic field. Finally, in the T04 model, this boundary depends on quasi-circular contours defined in the equatorial plane with a size depending on the dynamic pressure assumed. Since at the distance from which open field lines are detected in the three models the

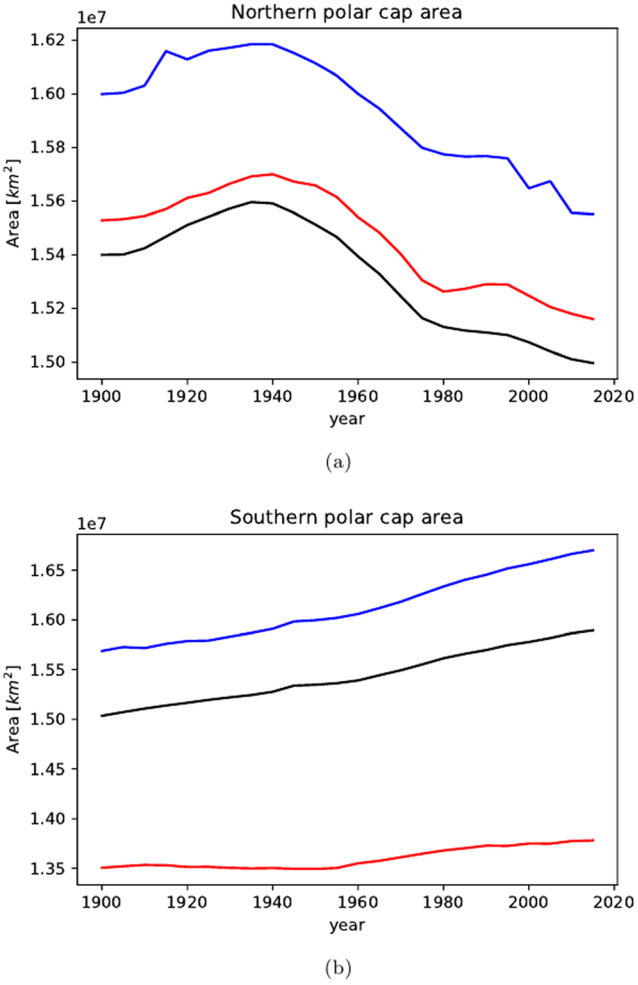

Figure 4. Polar cap areas for the (a) Northern and (b) Southern Hemisphere estimated with the constant intensity (black), superposition (blue), and the T04 (red) models.

dipolar component of the Earth's field is overwhelmingly dominant, the polar cap or auroral oval shapes, their center position and their relative areas SV are similar. However, the polar cap size varies: with the magnetopause distance in the constant intensity model, with the uniform external field value in the superposition model, and with the quasi-circular size in the T04 model. In summary, the similarity in the SV of the area based on all three models provides confidence in the robustness of the results.

The reason for the shrinking northern auroral oval is the effect of the SV of the nondipolar magnetic field components whose energy has been increasing at the dipole component expense (e.g., Amit & Olson, 2010). Before 1940 Earth's surface field at both poles has been weakening (Figures 5a and 5b), leading to a reduction in the distance to the magnetopause and expansion of the polar caps (Figure 2a). After 1940, in the southern polar region the intensity continued to drop (Figure 5d) and the polar cap continued to increase. In contrast, in the northern polar region since 1940 the intensity has been increasing (Figure 5c) hence the polar cap has been shrinking (Figure 2a).

What core field kinematics caused the surprising surface intensity increase and the subsequent polar cap area decrease at the north? As already noted in Figure 3, the SV of the nondipole field significantly affects the temporal variation of the polar cap area. Figure 6 shows two snapshots of the radial component of the Earth's magnetic field and its SV at the core-mantle boundary (CMB) below the northern hemisphere, one before and one after 1940. Because the surface field is mostly affected by low degrees, we examine in Figure 6 the field and its SV truncated at degree 5 while in Figure 7 we consider the full IGRF model until degree 13. In Figure 6 the field at the CMB in both epochs is dominated by two high-latitude flux patches, one below North America and the other below Siberia. This morphology mostly originates from spherical harmonic degree 2 (and order 2), which is the lowest nondipole degree, that is, its signature affects the field at the surface. Interpretations of local field and SV follow two end-member scenarios: Coincident field and SV structures indicate intensification (same sign) or weakening (opposite sign), whereas coincident field patch and a bipolar SV structure indicate drift (Amit, 2014). Accordingly, in 1920 the flux patch below North America is weakening while the flux patch below Siberia is drifting westward (Figures 6a and 6b), leading to a decrease in intensity in this period. In contrast, in 1980 the North America patch is drifting westward while the Siberia patch is strengthening (Figures 6c and 6d), leading to an increase in the intensity in this period at northern high latitudes. The recent intensification of the Siberian flux patch can also be traced when considering the full IGRF model (Figure 7). In 1920 positive SV correlates with this patch (Figures 7a and 7b); that is, it is locally weakening, whereas in 1980 a negative SV structure dominates this region (Figures 7c and 7d); that is, it is locally strengthening. Consequently, the SV of the two northern high-latitude flux patches culminated in the local surface field intensification and reduction in northern polar cap area.

Figures 8a and 8b show the field lines for the dipolar and nondipolar field, respectively. Figure 8c shows the field lines for the total field where red arrows indicate a more intense field and blue arrows a less intense field with respect to the pure dipole field. The contribution from multipolar components is positive in the northern polar region and negative in most of the southern, in agreement with a regional origin to polar caps SV.

4. Discussion and Conclusions

In a very first approximation, the open field lines determined by our constant intensity magnetopause model correspond to the tail lobe lines in a closed magnetosphere model, which are considered as the open field lines, since they do not cross the equatorial plane (Milan, 2009). Their footprints determine the polar

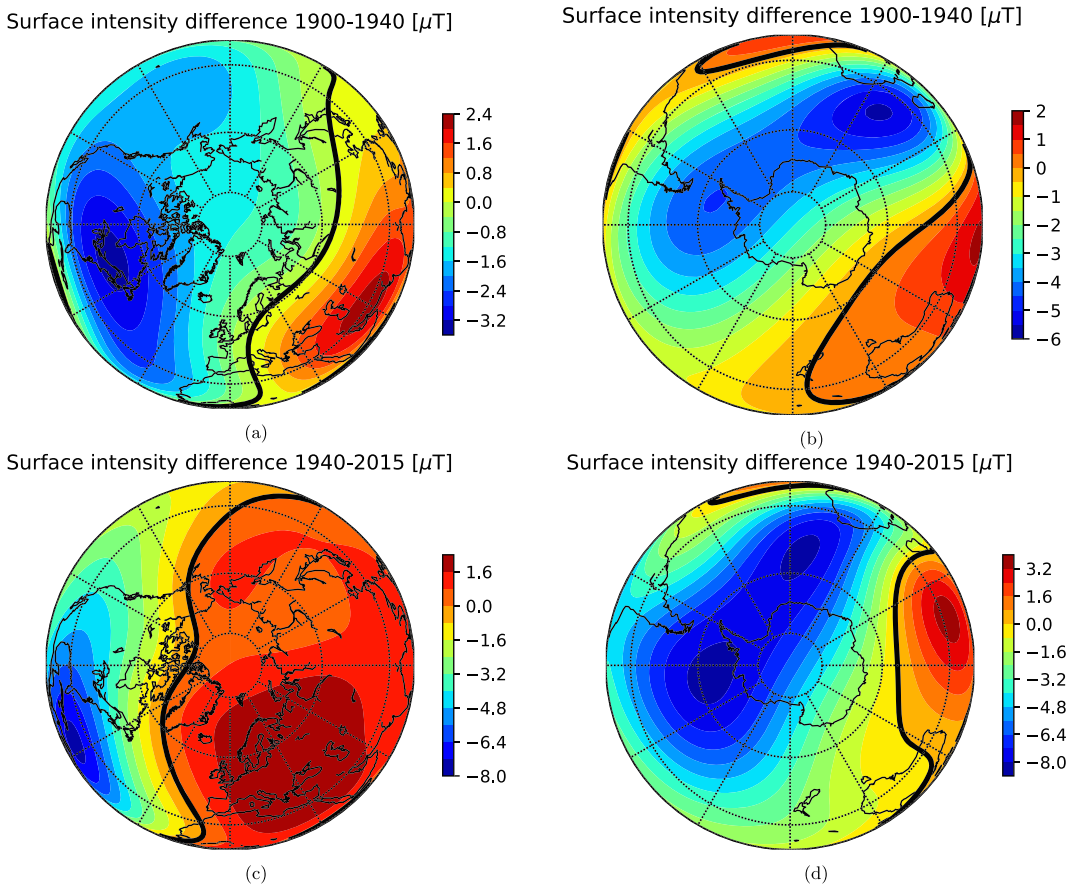

Figure 5. Intensity difference at Earth's surface (a) 1940–1900, Northern Hemisphere; (b) 1940–1900, Southern Hemisphere; (c) 2015–1940, Northern Hemisphere; and (d) 2015–1940, Southern Hemisphere.

caps. Our magnetopause model, therefore, acts as an "intermediary" approach to give fairly reasonable results for a "ground state" magnetosphere. This method is equivalent to that used by Oguti (1993) who estimated the variation of auroral zones (he uses "zone" as synonym of "oval" in this case) during a 1,000-yr period. He considered for the auroral zone inner limit (i.e., the polar cap boundary) the region connected to the apex magnetic field intensity that equals 49 nT. An advantage of our method is that a first approximation of the dayside magnetopause can be assessed for any magnetic field configuration.

According to scaling laws, which are rigorously valid under the hypothesis of self-similarity, the polar cap boundary latitude, λ_p, should vary in terms of the dipole moment, M, according to $\cos(\lambda_p) \propto (1/M)^{1/6}$ (Glassmeier et al., 2004; Siscoe & Chen, 1975; Vogt & Glassmeier, 2001) for a pure dipole magnetic field and a steady solar wind under quiet conditions (that is reasonable for a long-term average condition). This means that for the present-day decreasing M, λ_p should shift to lower latitudes with a consequent increasing area for both hemispheres. However, the SV of the polar cap geometric centers and areas in both hemispheres are in disagreement with these scaling laws. In particular, the northern polar cap geometric center has been drifting poleward (Figure 1) and its area has been decreasing since 1940 (Figure 2).

Our three considered magnetospheric models exhibit decent agreement in terms of the SV of the polar cap areas. We found in the three models a transition from temporal decrease in the surface intensity below northern high latitudes before 1940 (Figure 5a) to temporal increase of the intensity in this region thereafter (Figure 5c). The kinematic origin of this transition can be traced to the SV of particular geomagnetic flux

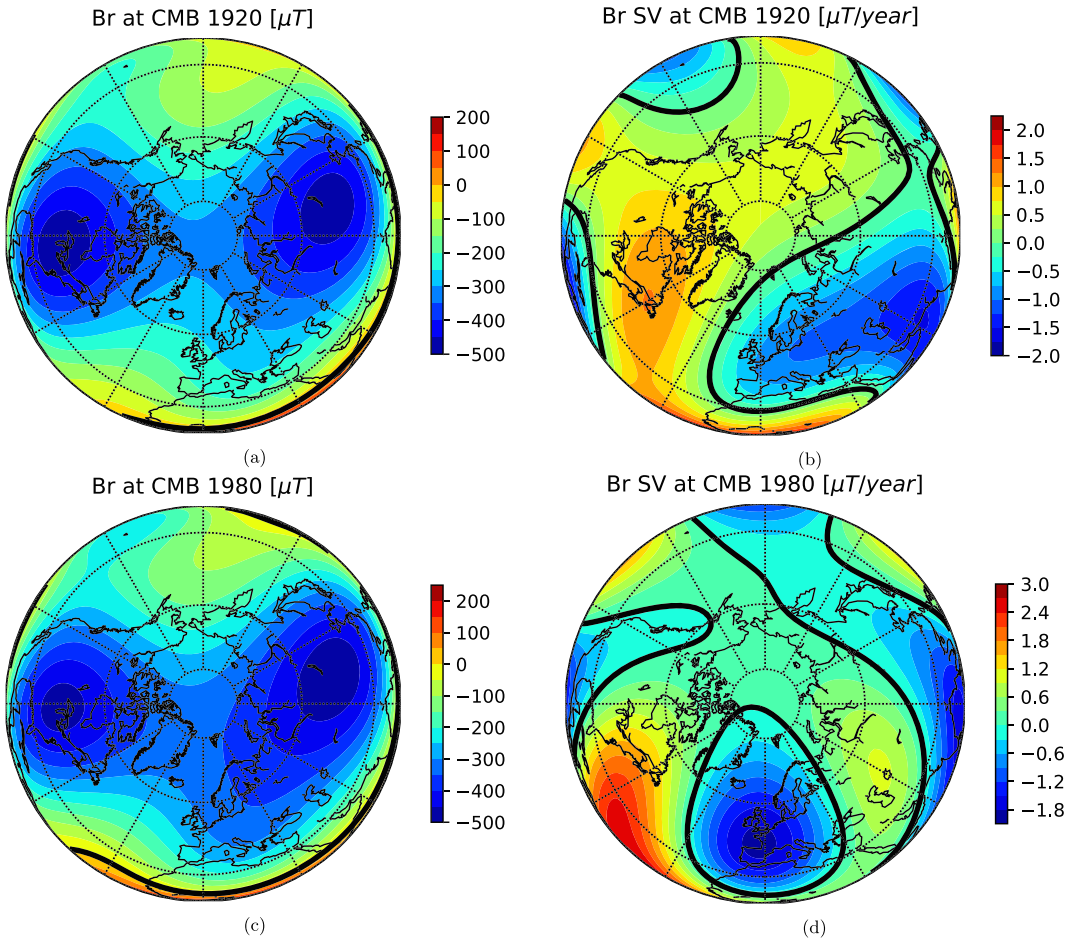

Figure 6. Radial geomagnetic field (a and c) and its SV (b and d) at the core-mantle boundary in 1920 (a and c) and 1980 (b and d) using IGRF-12 until spherical harmonic degree 5.

patches on the CMB (Figure 6). These recent SV features led to local intensification of the surface field at northern high latitudes and consequently reduction in the area of the northern polar cap (Figure 2).

The shrinking northern auroral zone originates from hemispheric differences in the geomagnetic field and consequently in the ionospheric conditions. Korte and Stolze (2016) mentioned that the northern auroral oval is more distorted at present than the southern oval, which they attributed to the nondipolar field components. Tsyganenko (2019) found that the northern polar cap moves faster than the southern (see Figure 1). These findings are in qualitative agreement with our results.

Solar activity long-term variation also affects the auroral oval size. Solar activity determines solar wind parameters, which in turn modifies the dynamic pressure at the magnetopause, directly determining the auroral oval size. However, this effect is equivalent for both auroral ovals, that is, an increase or decrease in size, displacing boundaries equatorward or poleward for increasing or decreasing solar activity levels respectively.

Comparison with observational data may validate our results. Available databases relevant for the auroral zone area include the Active Magnetosphere and Planetary Electrodynamics Response Experiment (AMPERE) (Milan et al., 2015) and the Defense Meteorology Satellite Program spacecraft (DMSP), or magnetometer data with the method described by Johnsen (2013). However, several difficulties render such a comparison nonstraightforward. First, different databases correspond to somewhat different physical areas (e.g., auroral zone and polar cap). Second, preliminary analyses of different databases give different results (not shown). Third, the observational databases cover too short periods (e.g., Johnsen, 2013; Kilcommons

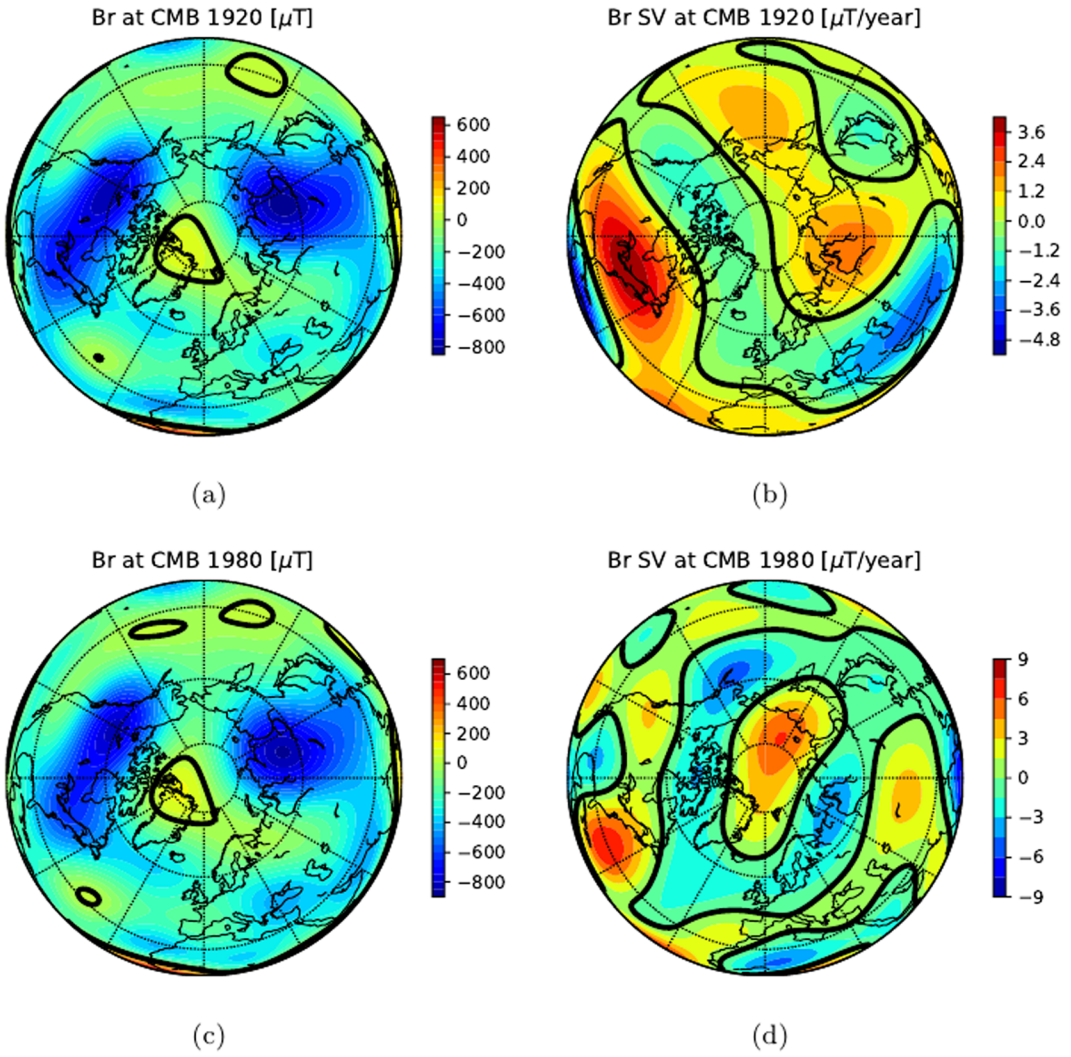

Figure 7. Radial geomagnetic field (a and c) and its SV (b and d) at the core-mantle boundary in 1920 (a and c) and 1980 (b and d) using full IGRF-12 until spherical harmonic degree 13.

et al., 2017) compared to the historical geomagnetic data covered, for example, by IGRF. Finally, the observations contain the solar activity contribution that has low-frequency variations compared to our SV analysis, in addition to a solar SV variation, that need to be properly filtered out in order to obtain reliable trends, which can be attributed only to the *internal* Earth's magnetic field. Indeed, investigation of the SV of the polar cap locations related to the Earth's magnetic field avoided comparison with such observations (Tsyganenko, 2019).

The shrinking northern auroral oval revealed here for the first time has important societal consequences. Within this smaller auroral oval, increased particle precipitation density might lead to increased damage to airplane and ship positioning systems, spacecraft electronic systems, and airline passengers when passing above the North Pole region. Continuous monitoring of Earth's magnetic field by surface observatories and dedicated satellites such as SWARM (Friis-Christensen et al., 2006), updated models of the core field (e.g., Gillet et al., 2015; Sabaka et al., 2015), improved modeling of the magnetospheric field (Cnossen, 2017; Tsyganenko & Andreeva, 2015) and interdisciplinary studies combining these models will reveal whether the current trend of shrinking northern auroral oval will persist.

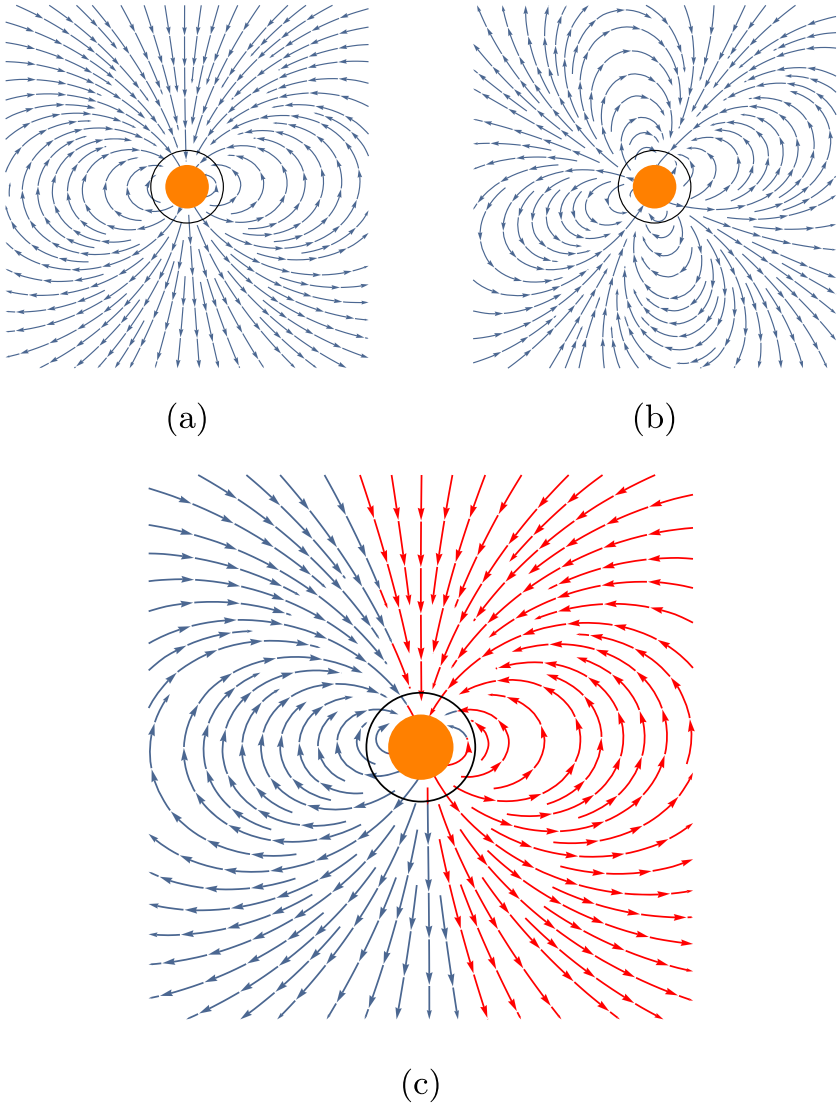

Figure 8. Field lines for (a) the dipolar, (b) nondipolar and (c) total field on the Greenwich meridian. In (c) an intensity increase is in red and an intensity decrease in blue with respect to the pure dipolar field. The black circle denotes Earth's surface and the orange disk is Earth's core.

Data Availability Statement

The data used in this work are available as supporting information of this work.

Acknowledgments

This work was supported by Projects PICT 2015-0511 and PIUNT E642. H. A. acknowledges financial support from program PNP of INSU. The models used in this work are as follows: Tsyganenko, IGRF, and magnetic field line tracer codes are in GeoPack-2008, freely available online (http://geo.phys.spbu.ru/~tsyganenko/Geopack-2008.html).

References

Akasofu, S. I. (1983). Evolution of ideas in solar-terrestrial physics. *Geophysical Journal of the Royal Astronomical Society*, *74*(1), 257–299. https://doi.org/10.1111/j.1365-246X.1983.tb01880.x

Amit, H. (2014). Can downwelling at the top of the Earth's core be detected in the geomagnetic secular variation? *Physics of the Earth and Planetary Interiors*, *229*, 110–121. https://doi.org/10.1016/j.pepi.2014.01.012

Amit, H., Coutelier, M., & Christensen, U. (2018). On equatorially symmetric and antisymmetric geomagnetic secular variation timescales. *Physics of the Earth and Planetary Interiors*, *276*, 190–201. https://doi.org/10.1016/j.pepi.2017.04.009

Amit, H., & Olson, P. (2008). Geomagnetic dipole tilt changes induced by core flow. *Physics of the Earth and Planetary Interiors*, *166*(3-4), 226–238. https://doi.org/10.1016/j.pepi.2008.01.007

Amit, H., & Olson, P. (2010). A dynamo cascade interpretation of the geomagnetic dipole decrease. *Geophysical Journal International*, *181*, 1411–1427. https://doi.org/10.1111/j.1365-246X.2010.04596.x

Aubert, J., Finlay, C. C., & Fournier, F. (2013). Bottom-up control of geomagnetic secular variation by the Earth's inner core. *Nature*, *502*(7470), 219–223. https://doi.org/10.1038/nature12574

Beard, D. B. (1960). Interaction of the solar plasma with the Earth's magnetic field. *Physical Review Letters*, *5*(3), 89–91. https://doi.org/10.1103/PhysRevLett.5.89

Bevis, M., & Cambareri, G. (1987). Computing the area of a spherical polygon of arbitrary shape. *Mathematical Geology*, *19*(4), 335–346. https://doi.org/10.1007/BF00897843

Busse, F. (1970). Thermal instabilities in rapidly rotating systems. *Journal of Fluid Mechanics*, *44*(3), 441–460. https://doi.org/10.1017/S0022112070001921

Carlowicz, M. J., & Lopez, R. E. (2002). *Storms from the Sun* (). Washington DC: Joseph Henry Press.

Christensen, U., & Tilgner, A. (2004). Power requirement of the geodynamo from ohmic losses in numerical and laboratory dynamos. *Nature*, *429*(6988), 169–171. https://doi.org/10.1038/nature02508

Cnossen, I. (2017). The impact of century-scale changes in the core magnetic field on external magnetic field contributions. *Space Science Reviews*, *206*(1-4), 259–280. https://doi.org/10.1007/s11214-016-0276-x

Feldstein, Y. I. (2016). The discovery and the first studies of the auroral oval: A review. *Geomagnetism and Aeronomy*, *56*(2), 129–142. https://doi.org/10.1134/S0016793216020043

Finlay, C. C., Aubert, J., & Gillet, N. (2016). Gyre-driven decay of the Earth's magnetic dipole. *Nature Communications*, *7*, 10422. https://doi.org/10.1038/ncomms10422

Finlay, C. C., & Jackson, A. (2003). Equatorially dominated magnetic field change at the surface of Earth's core. *Science*, *300*(5628), 2084–2086. https://doi.org/10.1126/science.1083324

Fraser-Smith, A. C. (1987). Centered and eccentric geomagnetic dipoles and their poles, 1600–1985. *Reviews of Geophysics*, *25*(1), 1–16. https://doi.org/10.1029/RG025i001p00001

Friis-Christensen, E., Lühr, H., & Hulot, G. (2006). Swarm: A constellation to study the Earth's magnetic field. *Earth, Planets and Space*, *58*(4), 351–358. https://doi.org/10.1186/BF03351933

Gillet, N., Barrois, O., & Finlay, C. C. (2015). Stochastic forecasting of the geomagnetic field from the COV-OBS.x1 geomagnetic field model, and candidate models for IGRF-12. *Earth, Planets and Space*, *67*(1), 71. https://doi.org/10.1186/s40623-015-0225-z

Gillet, N., Huder, L., & Aubert, J. (2019). A reduced stochastic model of core surface dynamics based on geodynamo simulations. *Geophysical Journal International*, *219*(1), 522–539. https://doi.org/10.1093/gji/ggz313

Glassmeier, K. H., & Vogt, J. (2010). Magnetic polarity transitions and biospheric effects. *Space Science Reviews*, *155*(1-4), 387–410. https://doi.org/10.1007/s11214-010-9659-6

Glassmeier, K. H., Vogt, J., Stadelmann, A., & Buchert, S. (2004). Concerning long-term geomagnetic variations and space climatology. *Annales Geophysicae*, *22*(10), 3669–3677. https://doi.org/10.5194/angeo-22-3669-2004

Gombosi, T. I., Powell, K. G., De Zeeuw, D. L., Clauer, C. R., Hansen, K. C., Manchester, W. B., et al. (2004). Solution-adaptive magnetohydrodynamics for space plasmas: Sun-to-Earth simulations. *Computing in Science & Engineering*, *6*(2), 14–35. https://doi.org/10.1109/MCISE.2004.1267603

Hill, T. W., & Rassbach, M. E. (1975). Interplanetary magnetic field direction and the configuration of the day side magnetosphere. *Journal of Geophysical Research*, *80*(1), 1–6. https://doi.org/10.1029/JA080i001p00001

Holme, R. (2015). Large-scale flow in the core. In P. Olson (Ed.), *Treatise on geophysics* (Second ed., Vol. 8, Chap. 8.04, pp. 91–113). Amsterdam: Elsevier Science.

Jackson, A., Jonkers, A., & Walker, M. (2000). Four centuries of geomagnetic secular variation from historical records. *Philosophical Transactions of the Royal Society of London A*, *358*(1768), 957–990. http://doi.org/10.1098/rsta.2000.0569

Jault, D. (2008). Axial invariance of rapidly varying diffusionless motions in the Earth's core interior. *Physics of the Earth and Planetary Interiors*, *166*(1-2), 67–76. https://doi.org/10.1016/j.pepi.2007.11.001

Johnsen, M. G. (2013). Real-time determination and monitoring of the auroral electrojet boundaries. *Journal of Space Weather and Space Climate*, *3*, A28. http://doi.org/10.1051/swsc/2013050

Kilcommons, L. M., Redmon, R. J., & Knipp, D. J. (2017). A new DMSP magnetometer and auroral boundary data set and estimates of field-aligned currents in dynamic auroral boundary coordinates. *Journal of Geophysical Research: Space Physics*, *122*, 9068–9079. https://doi.org/10.1002/2016JA023342

Korte, M., & Stolze, S. (2016). Variations in mid-latitude auroral activity during the Holocene*. *Archaeometry*, *58*(1), 159–176. https://doi.org/10.1111/arcm.12152

Lhuillier, F., Fournier, A., Hulot, G., & Aubert, J. (2011). The geomagnetic secular variation timescale in observations and numerical dynamo models. *Geophysical Research Letters*, *38*, L09306. https://doi.org/10.1029/2011GL047356

Lowes, F. (1974). Spatial power spectrum of the main geomagnetic field, and extrapolation to the core. *Geophysical Journal International*, *36*(3), 717–730. https://doi.org/10.1111/j.1365-246X.1974.tb00622.x

Milan, S. E. (2009). Both solar wind-magnetosphere coupling and ring current intensity control of the size of the auroral oval. *Geophysical Research Letters*, *36*, L18101. https://doi.org/10.1029/2009GL039997

Milan, S. E., Carter, J. A., Korth, H., & Anderson, B. J. (2015). Principal Component Analysis of Birkeland currents determined by the Active Magnetosphere and Planetary Electrodynamics Response Experiment. *Journal of Geophysical Research: Space Physics*, *120*, 10,415–10,424. https://doi.org/10.1002/2015JA021680

Oguti, T. (1993). Prediction of the location and form of the auroral zone: Wandering of the auroral zone out of high latitudes. *Journal of Geophysical Research*, *98*(A7), 11,649–11,655. https://doi.org/10.1029/93JA00328

Olson, P., & Amit, H. (2006). Changes in Earth's dipole. *Naturwissenschaften*, *93*(11), 519–542. https://doi.org/10.1007/s00114-006-0138-6

Riley, P., Baker, D., Liu, Y. D., Verronen, P., Singer, H., & Güdel, M. (2018). Extreme space weather events: From cradle to grave. *Space Science Reviews*, *214*, 21. https://doi.org/10.1007/s11214-017-0456-3

Sabaka, T. J., Olsen, N., Tyler, R. H., & Kuvshinov, A. (2015). CM5, a pre-Swarm comprehensive geomagnetic field model derived from over 12 yr of CHAMP, Ørsted, SAC-C and observatory data. *Geophysical Journal International*, *200*(3), 1596–1626. https://doi.org/10.1093/gji/ggu493

Schneider, P. J., & Eberly, D. H. (2003). Chapter 13—Computational geometry topics. In P. J. Schneider, & D. H. Eberly (Eds.), *Geometric tools for computer graphics*, *The Morgan Kaufmann Series in Computer Graphics* (pp. 673–825). Elsevier Science Inc.655 Avenue of the Americas New York, United States: Morgan Kaufmann.

Silverman, S. M. (1992). Secular variation of the aurora for the past 500 years. *Reviews of Geophysics*, *30*(4), 333–351. https://doi.org/10.1029/92RG01571

Siscoe, G. L., & Chen, C. K. (1975). The paleomagnetosphere. *Journal of Geophysical Research*, *80*(34), 4675–4680. https://doi.org/10.1029/JA080i034p04675

Stern, D. P. (1973). A study of the electric field in an open magnetospheric model. *Journal of Geophysical Research*, *78*(31), 7292–7305. https://doi.org/10.1029/JA078i031p07292

Thébault, E., Finlay, C. C., Beggan, C., Alken, P., Aubert, J., et al. (2015). International Geomagnetic Reference Field: The 12th generation. *Earth, Planets and Space*, *67*(1), 79. https://doi.org/10.1186/s40623-015-0228-9

Tsyganenko, N. A. (2019). Secular drift of the auroral ovals: How fast do they actually move? *Geophysical Research Letters*, *46*, 3017–3023. https://doi.org/10.1029/2019GL082159

Tsyganenko, N. A., & Andreeva, V. A. (2015). A forecasting model of the magnetosphere driven by an optimal solar wind coupling function. *Journal of Geophysical Research: Space Physics*, *120*, 8401–8425. https://doi.org/10.1002/2015JA021641

Tsyganenko, N. A., & Sitnov, M. I. (2005). Modeling the dynamics of the inner magnetosphere during strong geomagnetic storms. *Journal of Geophysical Research*, *110*, A03208. https://doi.org/10.1029/2004JA010798

Vogt, J., & Glassmeier, K. H. (2001). Modelling the paleomagnetosphere: Strategy and first results. *Advances in Space Research*, *28*, 863–868. https://doi.org/10.1016/S0273-1177(01)00504-X

Winkler, H., Sinnhuber, M., Notholt, J., Kallenrode, M. B., Steinhilber, F., Vogt, J., et al. (2008). Modeling impacts of geomagnetic field variations on middle atmospheric ozone responses to solar proton events on long timescales. *Journal of Geophysical Research*, *113*, D02302. https://doi.org/10.1029/2007JD008574

Zossi, B. S., Fagre, M., Amit, H., & Elias, A. G. (2019). Polar caps during geomagnetic polarity reversals. *Geophysical Journal International*, *216*(2), 1334–1343. https://doi.org/10.1093/gji/ggy494